

## The Metallurgy of Alloy 625

Stephen Floreen, Gerhard E. Fuchs, and Walter J. Yang

Knolls Atomic Power Laboratory  
P. O. Box 1072  
Schenectady, New York 12301-1072

### Abstract

The objective is to describe the effects of alloy composition and processing history on the microstructure and properties of Alloy 625. This includes discussion of the solidification behavior, the precipitation of different carbides, and Delta, Laves and  $\gamma$ " phases. The paper will show how various properties can be optimized by tighter control of alloy chemistry and processing steps.

## INTRODUCTION

Alloy 625 is a highly alloyed nickel-base alloy that can provide high strength, corrosion resistance in a variety of environments, and good fabricability and weldability. Because of this attractive combination of properties, Alloy 625 has found wide-spread applications.

Table I gives the nominal composition range for Alloy 625. The high levels of Cr and Mo provide good corrosion resistance plus strength, while Fe and Nb provide further solid solution strengthening. The Al and Ti additions are principally for refining purposes and are kept low compared to Alloys like 718 to enhance weldability. However, as discussed below, with sufficient (Nb + Ti + Al) content precipitation hardening by  $\gamma''$  can be achieved in Alloy 625.

This review will first look at the solidification behavior of Alloy 625 compositions, since this directly impacts the properties of castings and weldments, and can significantly influence the microstructure in wrought products. This section will be followed by a description of the various phase transformations that can take place as a function of time, temperature, and composition.

One of the principal messages that will come out of this review is that the composition range shown in Table I is overly broad. Depending upon the product form, and the desired properties, tighter control of the composition often can be used to help ensure more consistent properties between different heats of Alloy 625. As is usually the case when composition adjustments are made, however, a change that is helpful for one property may be deleterious to some other property. Some of these trade-offs in composition versus properties will be discussed in the paper.

Table I

Alloy 625 Composition

Ni	Cr	Fe	Mo	Nb (+ Ta)	C	Mn	Si	Al	Ti
58.0 min	20.0 - 23.0	5.0 max	8.0 - 10.0	3.15 - 4.15	0.10 max	0.50 max	0.50 max	0.40 max	0.40 max

## SOLIDIFICATION BEHAVIOR

Alloy 625 can be considered to a useful degree to be a modification of Alloy 718. This approximation is especially helpful in terms of understanding the solidification behavior, since the extensive work that has been done on that alloy can be used to advantage to help describe the general features observed in Alloy 625.

The dominating solidification reaction in both alloys is the enrichment of the remaining interdendritic liquid in niobium, and the consequent formation of niobium-rich Laves phase and/or niobium carbide during the final stages of solidification. Figure 1 shows that pseudo-binary phase diagram for Alloy 718 originally proposed by Eiselstein (Reference 1) to explain the enrichment of the remaining liquid in Nb (and Ta) and the resultant formation of  $A_2B$  Laves phase. Detailed versions of this diagram have been developed by more recent investigators, but the principal feature in all cases is the increased Nb content in the final liquid to solidify.

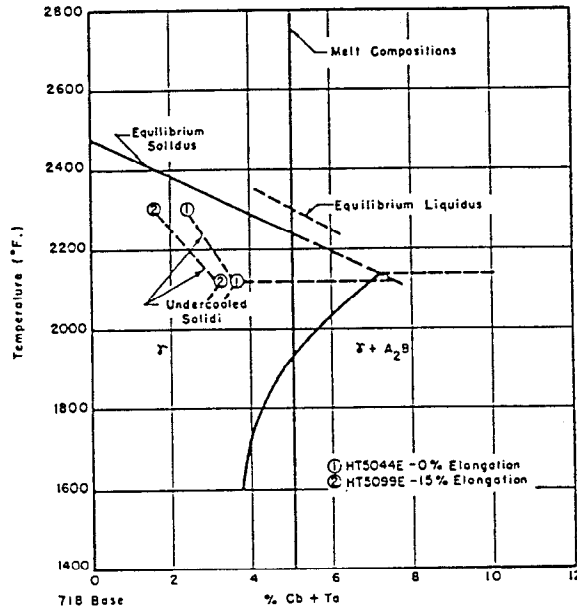


Figure 1. Pseudo-Equilibrium Solidification Diagram for Alloy 718 Showing Formation of  $A_2B$  Laves Phase During Solidification (Reference 1)

For present purposes, a better way to view the solidification is shown in Figure 2 in a pseudo ternary equilibrium diagram. This is a schematic representation based on the Alloy 718 diagram proposed by Radhakrishnan and Thompson (Reference 2). As shown in Figure 2, the C/Nb ratio dictates the solidification path and the resultant microstructures. Three different paths can be followed. Path 1, at high C/Nb ratios, leads to the formation of  $\gamma + NbC$  with no Laves phase. Path 2, at intermediate C/Nb ratios, leads first to  $\gamma + NbC$ , followed by Laves phase formation at the end of solidification. Path 3, at low C/Nb ratios leads to  $\gamma + Laves$  with no NbC.

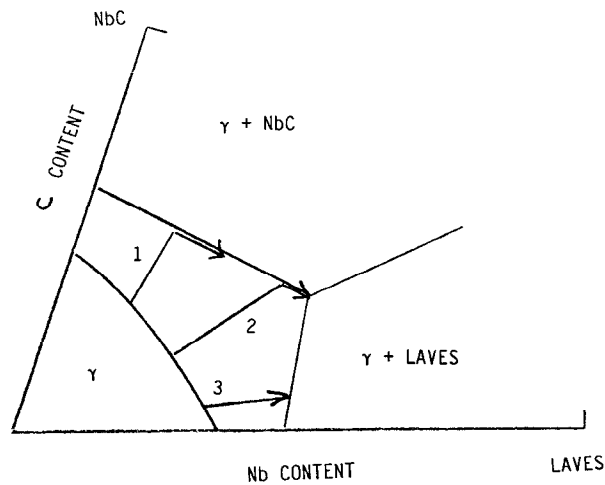


Figure 2. Schematic View of Solidification Paths in A625

Examinations of the microstructures in Alloy 625 heats generally appear consistent with the compositional effects shown in Figure 2. In typical heats Path 1 or Path 2 microstructures are observed, i.e., with NbC or with NbC + Laves particles. However, a well-defined C/Nb value at which the solidification changes from Path 1 to Path 2 is not apparent from these examinations. This doubtless reflects the fact that the solidification rate and other alloy chemistry variations also affect the microstructure in addition to the C/Nb ratio. Path 3 microstructures, without NbC particles, are not common but have been seen in Alloy 625 heats containing less than 0.01% C (Reference 3).

The iron content also affects the solidification structure. In cast heats of Alloy 718, lowering the Fe content reduced the amount of Laves phase (Reference 4). Reducing the iron and silicon contents in Alloy 625 welding filler wire has also been helpful to the ductility in weldments because the formation of Laves phase is minimized. Table II compares the properties of heavy section gas tungsten arc weldments made with a standard chemistry wire and with a low iron and silicon wire. Significant quantities of Laves phase and NbC particles were observed in the interdendritic regions of the weld metal made with the standard filler wire, but not in the weld made with the low Fe and Si filler wire. The significant improvement in toughness appears to be due primarily to this change in microstructure.

Table II

Comparison of Impact Properties and Weld Metal Compositions Using Standard Alloy 625 Wire and Low Fe and Low Si Wire

Filler Wire	Test Temp.	Charpy V-Notch Impact Energy
Standard	RT	42.3
	-320°F	37.2
Low Fe & Low Si	RT	152.7
	-320°F	127.7

Weld Metal Chemistries

Weld Metal	Fe	Si	Ti	Mn	Al	C	Cr	Mo	Nb
Standard	3.19	0.22	0.16	0.17	0.25	0.03	22.1	8.88	3.76
Low Fe & Si	0.80	0.08	0.23	0.14	0.28	0.02	21.5	8.64	3.49

The influence of iron on the solidification behavior can be shown schematically by another pseudo-ternary diagram, adapted from studies of Alloy 718 (Reference 5). Figure 3 shows this diagram, in terms of the trace of the solidification path moving from the  $\gamma$  to the  $\gamma + A_2B$  Laves particles. Higher levels of Fe (or Cr) shift the solidification path downward and to the left in Figure 3, and thus increase the amounts of Laves phase formed during solidification.

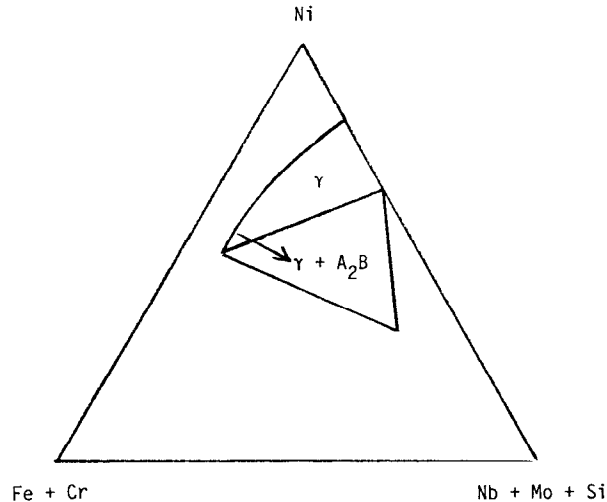


Figure 3. Pseudo-Equilibrium Ternary Solidification Diagram for A718 Showing Solidification Path Direction from  $\gamma$  to  $\gamma + A_2B$  Laves Phase (After Reference 5)

Figure 3 also indicates that higher levels of Nb, Mo, and Si promote the formation of Laves phase. This is consistent with chemical analyses of Laves phase particles in heats of Alloy 625. Laves phases are hexagonal close packed  $A_2B$  compounds that are found in a number of binary alloys. In more complex alloys, however, Laves particles can contain significant amounts of other alloying or impurity elements, and depart considerably in composition from a simple  $A_2B$  type chemistry. Table III gives the compositions of the Laves particles found in three different product forms of Alloy 625, banded plate stock, weld metal, and originally Laves-free plate stock that was heat treated for 48 hours at 1600°F. The results are given in atomic percent units. There are noticeable compositional variations between the three materials, that likely reflect the differences in processing history of the materials in which the particles were formed. In all cases, however, the Laves phase was significantly enriched in Nb, Mo, and Si, while the Fe, Cr, and Ni levels were not noticeably enriched versus the nominal Alloy 625 composition.

Also included in Table III are the compositions of Laves particles found in various Alloy 625 GTA welds by Cieslak (Reference 6) and in Alloy 625 weld metal made by three different weld processes by Wilson et al (Reference 7). The ranges of compositions found by these two investigations are shown in Table III, and further illustrate the considerable variability in composition found in Laves particles.

Cieslak, et al, (Reference 8) have reported similar composition trends in the Laves particles in heats of Alloys 718, 909, and a precipitation hardened version of Alloy 625 called Custom Aged Alloy 625. Additional compositional studies reported in References 9-11 indicate that B and Ti also promotes Laves phase, while Mg additions minimize Laves formation.

Table III

Chemical Compositions of Laves Phase Particles in Atomic Percents from Different Alloy 625 Materials

Element	Banded Plate Stock	Base Plate Heat Treated 48 Hrs at 1600°F	6 Inch GTA Weldment	GTA Welds Cieslak Reference 6	Three Weld Processes Wilson et al Reference 7
Ni	38	41	48	45.6-48.2	20.3-40.5
Cr	17	20	22	13.6-15.6	12.4-18.3
Mo	23	21	12	17.6-19.8	13.6-18.6
Nb	19	6	11	16.8-19.2	12.2-27.5
Fe	3	5	3	0.9-1.4	6.9-12.9
Si	6	6	4	0-2.2	6.1-9.7

The compositions of the NbC particles in various Alloy 625 weldments also have been reported (Reference 8). These are given in Table IV. Note that both blocky carbides and a dendritic Chinese script morphology at the grain boundaries were found. Also included in Table IV are the chemistries of blocky NbC particles found in wrought Alloy 625 samples by two different investigations (References 12 and 13). The carbides are primarily (Nb, Mo)C, with minor amounts of Ni and Cr present.

Table IV

Composition of NbC Particles (wt %) Reported in Literature

Ref.	Material	Fe	Ni	Cr	Nb	Mo	Ti
8	GTA Welds	0-0.4	0.1-4.1	1.3-7.4	65.0-82.6	4.4-13.2	--
	Blocky NbC Dendritic NbC	0.1-0.3	2.1-4.5	4.1-8.6	60.0-73.4	6.5-17.6	
12	625 Bar	---	2.6	1.2	89.3	2.8	4.0
13	Wrought 625 900°C/1 Hr	---	---	3.6	79.7	20.1	--
	Wrought 625 940°C/100 Hr	---	6.7	3.6	79.7	4.4	

In common with other similar nickel-base alloys, the tendency to form NbC and Laves phases during solidification causes inherent limitations on melt practices for Alloy 625. The melting procedure, i.e., AOD vs. VIM vs. ESR, etc., and the ingot size taken together limit the maximum heat size that will have an acceptable structure. This limit is not well defined for Alloy 625, but for current ESR melts the maximum practical ingot size appears to be about 40,000 pounds.

Even in much smaller heats, or in weldments, the preceding discussion indicates that using compositions with lower levels of elements such as Nb, Fe, and Si could be advantageous. To further explore the effects of

composition on the solidification behavior, differential thermal analysis (DTA) has been used to determine the liquidus and solidus temperatures during cooling for a series of Alloy 625 with systematic chemistry variations.

Table V gives the compositions of a set of 100 pound vacuum induction melts that were used for this investigation. The DTA tests were conducted on samples weighing approximately two grams that were heated and cooled at a nominal rate of 20°C per minute. Tungsten was used as a reference material. The test method generally follows that used by Cieslak and co-workers (References 3, 6 and 8) and the results generally appear consistent with the compositional effects they see in Alloy 625 and other similar alloys.

Table V  
Chemical Compositions of A625 Heats Used For DTA Tests

<u>C</u>	<u>Mn</u>	<u>Fe</u>	<u>Cr</u>	<u>Al</u>	<u>Ti</u>	<u>Mg</u>	<u>Co</u>	<u>Mo</u>	<u>Nb</u>	<u>B</u>	<u>N</u>
.008	.047	4.32	22.16	.27	.16	.014	.103	8.92	3.62	.0017	---
.018	.040	4.32	22.13	.26	.16	.013	.111	8.90	3.62	.0014	---
.026	.049	4.31	20.13	.27	.16	.012	.104	8.91	3.62	.0015	---
.046	.047	4.34	22.16	.27	.16	.015	.104	8.90	3.63	.0015	---
.068	.048	4.31	22.16	.27	.16	.013	.106	8.88	3.64	.0014	---
.021	.045	.053	22.04	.27	.15	.015	.121	8.88	3.64	.0014	---
.025	.047	4.28	21.96	.27	.155	.0093	.111	8.12	3.66	.0012	---
.028	.080	4.31	21.95	.27	.16	.014	.104	8.92	3.79	.0180	---
.029	.043	4.34	22.22	.26	.16	.028	.104	8.75	3.64	.0012	.10
.028	.045	4.34	22.15	.21	.155	.013	.106	8.88	3.07	.0015	---
.027	.044	4.31	22.14	.26	.025	.011	.107	8.90	3.64	.0014	---

Figure 4 shows the results in terms of the solidification range (liquidus temperature minus solidus temperature) during cooling versus the carbon content of the heats. The curve in the figure is drawn thru the data for the heats with different carbon contents. Increasing carbon significantly increased the solidification range. Very similar effects of C on the solidification range of Alloy 625 were observed by Cieslak (Reference 6). The effects of other individual alloying element variations are also shown. Increasing boron to 0.018% markedly increased the solidification range, because of the commonly observed effect of boron reducing the solidus temperature. A higher nitrogen content (0.10%) had surprisingly little effect. Reducing the Ti, Nb, Mo, and Fe contents to values approaching the lower limits for these elements in Table I tended to reduce the solidification range. Cieslak (Reference 6) also found that minimizing Si significantly reduced the solidification range.

Cieslak found that lowering the solidification range minimized the tendency for hot cracking during welding (Reference 6). Reducing the solidification range should minimize the amount of segregation that would take place during solidification and, therefore, improve the hot workability. Thus, reducing the C and Nb contents would be beneficial in reducing the amount of material available to form NbC or Laves phase, and also in reducing the

segregation of these elements during solidification. Decreasing the solidification range also may be part of the beneficial effect of reducing the iron content in minimizing Laves formation in weldments.

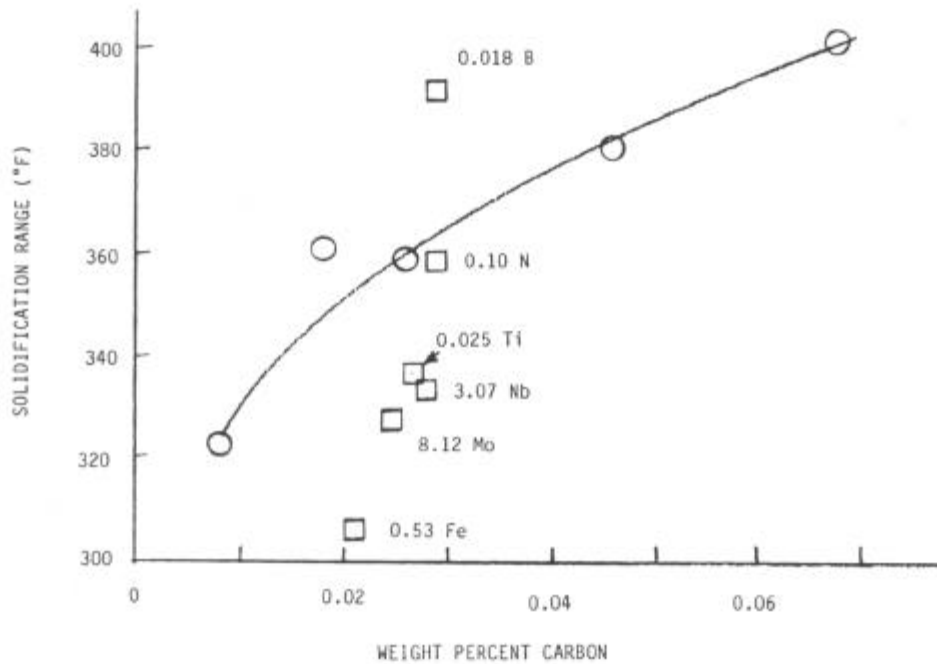


Figure 4. Solidification Range During Cooling of A625 Heats

If an ingot containing excessive Laves and/or NbC particles is hot worked to plate these particles can become strung out in planes parallel to the plate surface to give a banded microstructure. Figure 5 shows an example of a badly banded microstructure with high local concentrations of Laves phase particles found in some Alloy 625 plate stock. Layered microstructures of this type may have acceptable properties when deformed in directions parallel to the bands, but can display very poor ductility when strained perpendicular to bands. The material shown in Figure 5, for example, showed extensive cracking along the banded regions after the plate had been deformed to about 20% outer fiber strain by bending.



Figure 5. Photograph of Banded Microstructures in A625 Plate (425X)



As discussed below, Laves phase particle can be eliminated by solution annealing at high temperatures. Thus, suitable hot working and annealing practices can get rid of Laves particles in wrought products and the rather flagrant example described above should not be considered typical. However, NbC particles are much more stable and once formed are probably impossible to eliminate by conventional processing steps. Here also suitable hot working practices can usually produce wrought products with reasonably uniform non-localized distributions of NbC. However, high local concentrations of NbC in banded microstructure can be found in wrought products. Bands of carbide particles also will degrade the ductility in directions transverse to the bands, although the loss in ductility due to carbides does not appear nearly as severe as that resulting when Laves particles are present.

Bands of carbides also can cause problems during welding because of liquation of the carbides in the heat affected zone of the weldment. This has been examined by using a thermo-mechanical testing device (Gleeble) to produce five second thermal exposures at various temperatures in Alloy 625 plate stock containing bands of carbide particles.

Following this short time thermal pulse, the samples were heat treated at 1600°F. This latter heat treatment was used to delineate where the carbide particles had dissolved. When NbC particles liquate, the resultant liquid is highly concentrated in Nb and Mo. When this liquid solidifies on cooling, it forms a solid solution very rich in Nb and Mo that will then precipitate Delta phase particles when heat treated at 1600°F. The acicular shape of the Delta provides a distinctive needle-like morphology that is easy to identify, and marks the regions where NbC particles had liquated. Figure 6 shows examples of these localized patches of Delta in a specimen exposed at 2300°F for five seconds.

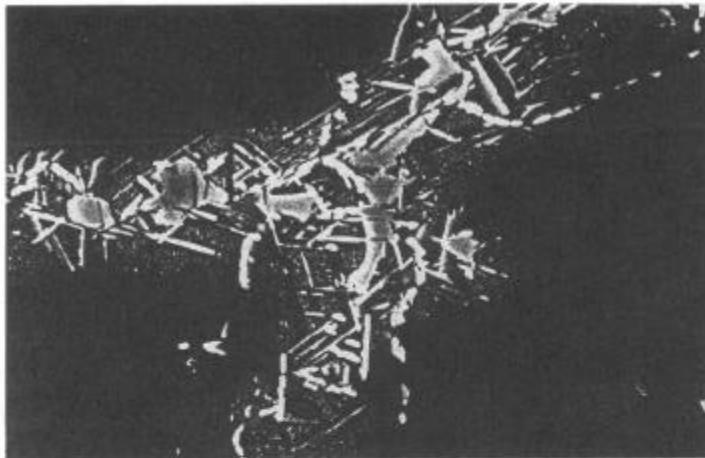


Figure 6. Delta Phase Particles Marking Locations of Liquated NbC Particles

Using this marking technique, a set of samples were examined to look for signs of liquation after five second thermal exposures at various temperatures. The results indicated that liquation of the NbC particles began at temperatures in the 2175-2200°F range, and became much more extensive at higher temperatures. It was also evident that liquation could be very extensive in banded regions that contained high concentrations of

NbC particles. Hence banded regions would be much more likely to form cracks during welding than materials in which the NbC particles were more uniformly distributed. It is also clear that applied or thermal stresses perpendicular to the bands would have much more severe effects than stresses parallel to the bands.

This constitutional liquation of the NbC particles takes place at temperatures on the order of 150°F below the bulk solidus temperatures observed during heating in the DTA tests. The localized melting can be explained in terms of the Path 1 and Path 2 solidification paths shown in Figure 2. If one plotted a vertical section through the first leg of either path, it would look schematically as shown in Figure 7; i.e., as a pseudo-binary eutectic between the  $\gamma$  matrix and NbC. Upon heating, when the NbC particles locally come into equilibrium with the (Nb + L) field, they will begin to melt. The present results indicate that this eutectic temperature is in the range of 2175-2200°F.

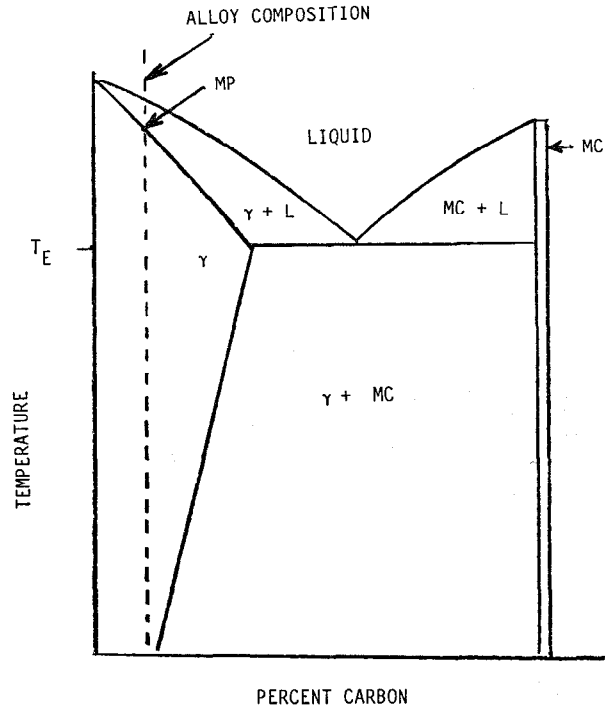


Figure 7. Pseudo Phase Diagram Showing Lower Temperature Eutectic in Equilibrium With MC Phase

In summary, the formation of Laves phase and/or NbC particles plays a major role in the solidification of Alloy 625. There are no obvious benefits to the presence of either of these phases in the final microstructure, and there are clearly detrimental effects if excessive or highly localized concentrations of these particles are present. Melting to lower levels of Nb and C, as well as lower levels of Fe, Mo and Si, would be helpful in minimizing the formation of these phases. The resultant benefits would probably be greatest in castings and weldments. In wrought products Laves particles could be eliminated and NbC particles at least left in reasonably non-localized distributions by suitable hot working and heat treating procedures. The need to prevent the formation of these phases during ingot solidification is correspondingly less critical.

## PHASE TRANSFORMATIONS

In this section, the phase changes that occur in Alloy 625, as a function of time and temperature, will be discussed. The starting material is solution annealed so that all phases, except the primary NbC particles discussed above, have been put into solid solution.

Several time-temperature-transformation (T-T-T) diagrams have been presented for Alloy 625. These differ somewhat from each other, and also from the proposed T-T-T diagram that will be described below. There are several possible reasons for these discrepancies, and it is not possible at this stage to clearly identify the reasons for the differences in the various diagrams. However, two factors will be discussed that illustrate why there can be noticeable variations in T-T-T diagrams for what is ostensibly the same alloy. The first is simply that variations in composition within the ranges given in Table I can significantly affect the T-T-T behavior and thus two different heats of Alloy 625 can give surprisingly different results. Examples of some of these compositional effects will be described.

A second source of variability is experimental, and involves the techniques used to identify the phases. One example described below is that Laves particles can form at grain boundaries that may be very difficult to distinguish from grain boundary carbides by optical metallographic examinations.

With these caveats in mind, Figure 8 presents the T-T-T diagram for nominal heats of wrought A625. Nominal in this case is defined by the chemistry ranges given in Table VI, which are typical of the compositions commonly found in commercial heats of Alloy 625 made in this country in recent years.

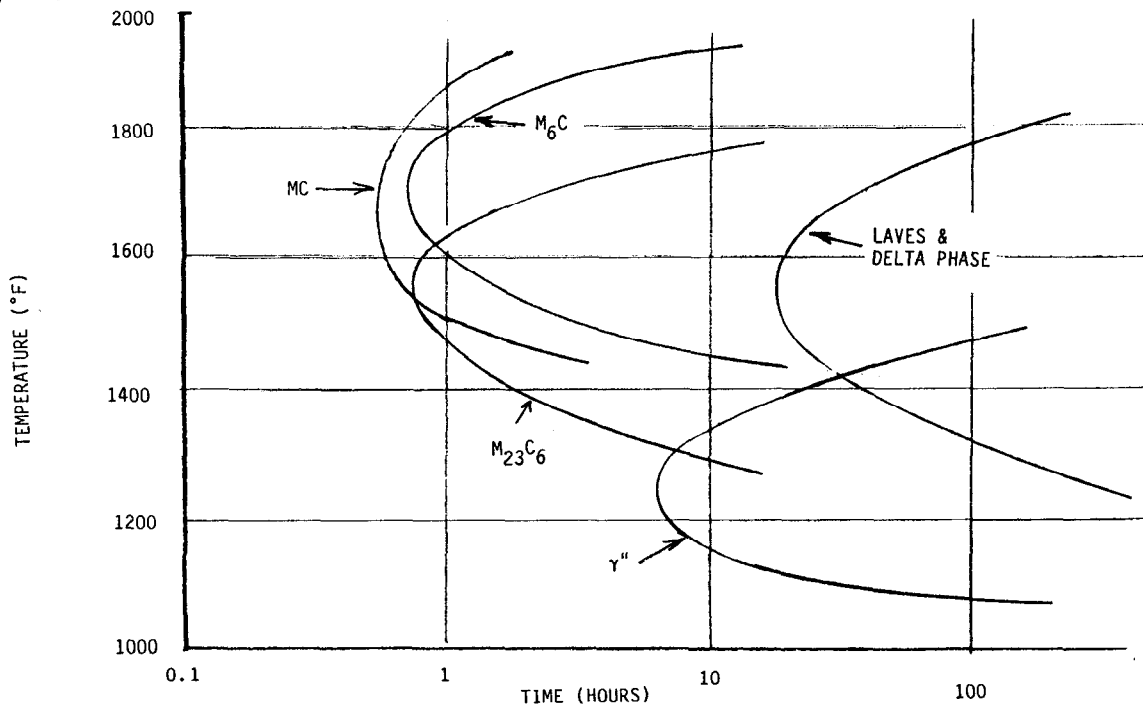


Figure 8. Approximate Time-Temperature-Transformation Diagram for Phases Forming at High Temperatures in A625

Table VI

Typical Chemistry Ranges for Commercial Alloy 625 Wrought Stock

Ni	Cr	Fe	Mo	Nb (+ Ta)	C	Mn	Si	Al	Ti
58.0 min	20.5 - 22.5	4.0 - 4.5	8.1 - 8.9	3.4 - 3.7	0.01 - 0.04	0.02 - 0.10	0.05 - 0.10	0.02 - 0.03	0.1 - 0.25

As indicated in Figure 8, a number of different carbides and intermetallic compounds can precipitate in A625 after thermal exposures, for times on the order of 0.1 to 100 hours. Still further changes, as discussed below, will occur with more prolonged exposures.

Table VII summarizes the crystal structures and typical compositions in atomic percent values of these phases. Note that the composition data are partitioned in this table by crystallographic position. Thus, in the case of the  $A_2B$  Laves phase, the Cr, Fe, and Ni are assumed to occupy the A positions in the crystal structure, and Si, P, Nb, and Mo occupy the B positions. As discussed before, there are two different NbC morphologies: the blocky shape that forms during solidification, and the dendritic form reported in weldments and also seen as a thin grain boundary film after heat treating wrought material.

Three different carbides can precipitate in wrought A625 grain boundaries. The positions of the noses of the various carbide curves in the T-T-T diagram are not well defined, but are on the order of 10 minutes. In practice, even fairly large sized cross-sections of nominal chemistry wrought Alloy 625 will not show grain boundary carbides after air cooling from solution annealing. Thus, if desired, grain boundary carbide precipitation can be easily suppressed during processing. The type of carbide formed during heat treating depends upon the temperature. At higher temperatures, roughly from 1600 to 1900°F, the carbides are both NbC as thin grain boundary films, and  $M_6C$ , where M is principally Ni, Cr, and Mo. At temperatures in the 1300-1600°F range, the grain boundary carbides are primarily  $M_{23}C_6$ , where M is almost entirely Cr. After intermediate temperature heat treatments, all three carbides usually can be found, as shown in Figure 9. The  $M_6C$  and  $M_{23}C_6$  carbides commonly have blocky, irregular shapes and form as series of separate, discrete grain boundary particles.

The precipitation of grain boundary carbides has been found to be sensitive to the Si content as well as the carbon content. Figure 10 shows the relative amounts of grain boundary carbides seen in a number of Alloy 625 heats after heat treating for 8 hours at 1600°F. At higher carbon levels, above about 0.035%, Si had no effect. At lower carbon levels, however, carbide precipitation was significantly retarded when the Si contents were below approximately 0.15%. The reason for this strong effect of Si is not clear. It may be noted in Table VII, and also in the results in Reference 11, that  $M_6C$  carbides in Alloy 625 contain about 5 wt % Si. This suggests that Si might promote the nucleation of  $M_6C$ , but further work is needed to establish the mechanism. In the practical sense, the results provide a good illustration of how a minor change in chemistry can significantly perturb the phase transformation behavior.

Table VII

Structures and Typical Compositions of the Precipitate Phases  
Which Occur in A625 During Thermal Exposures

Phase	Structure	Typical Composition
MC	Cubic, Fm3m $a_o = 0.43$ nm	Matrix blocky MC (Ti <sub>0.07</sub> Cr <sub>0.04</sub> Fe <sub>0.02</sub> Ni <sub>0.09</sub> Nb <sub>0.75</sub> Ni <sub>0.03</sub> )C (Ti <sub>0.53</sub> Cr <sub>0.03</sub> Ni <sub>0.04</sub> Nb <sub>0.39</sub> Mo <sub>0.01</sub> )C G.B. MC (Ti <sub>0.15</sub> Cr <sub>0.04</sub> Fe <sub>0.01</sub> Ni <sub>0.08</sub> Nb <sub>0.67</sub> Mo <sub>0.01</sub> )C
M <sub>6</sub> C	Cubic, Fd3m $a_o = 1.13$ nm	(Cr <sub>0.21</sub> Fe <sub>0.02</sub> Ni <sub>0.37</sub> Nb <sub>0.08</sub> Mo <sub>0.24</sub> Si <sub>0.08</sub> ) <sub>6</sub> C
M <sub>23</sub> C <sub>6</sub>	Cubic, Fm3m $a_o = 1.08$ nm	(Cr <sub>0.85</sub> Fe <sub>0.01</sub> Ni <sub>0.07</sub> Mo <sub>0.07</sub> ) <sub>23</sub> C <sub>6</sub>
γ''	Ord Tet, I4/mmm $a = 0.36$ , $c = 0.74$ nm	Ni <sub>3</sub> (Nb <sub>&gt;0.5</sub> Ti <sub>&lt;0.5</sub> Al <sub>&lt;0.5</sub> )
δ	Orth, Pmmm $a = 0.51$ , $b = 0.42$ $c = 0.45$	Ni <sub>3</sub> Nb
Laves	Hex, P6 <sub>3</sub> mmc $a = 0.47$ , $c = 0.77$ nm	(Cr <sub>0.31</sub> Fe <sub>0.08</sub> Ni <sub>0.41</sub> ) <sub>2</sub> (Si <sub>0.17</sub> Ti <sub>0.01</sub> Nb <sub>0.19</sub> Mo <sub>0.63</sub> )
(Cr, Nb) <sub>2</sub> N	Tet, P4/nmm $a = 0.3$ , $c = 0.77$ nm	(Cr <sub>0.39</sub> Ni <sub>0.07</sub> Nb <sub>0.41</sub> Mo <sub>0.13</sub> ) <sub>2</sub> N

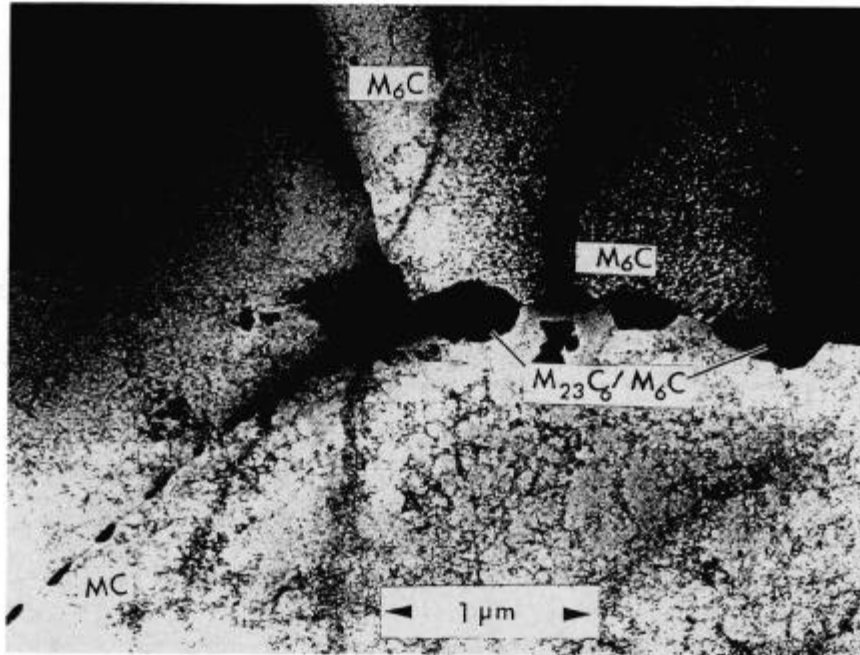
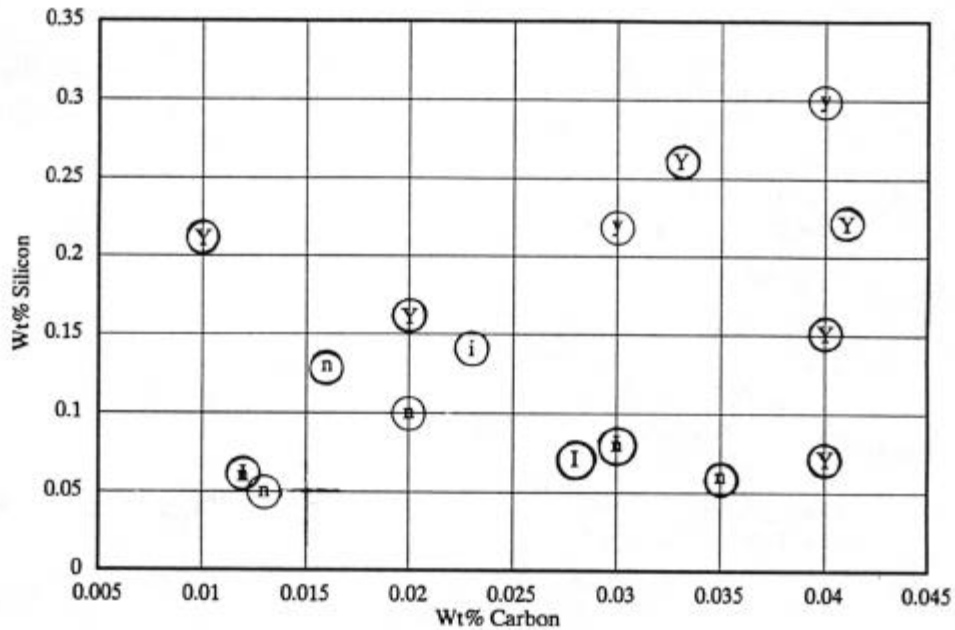


Figure 9. TEM Photograph of Grain Boundary Carbides in A625 After 8 Hours at 1600°F



y = GB carbide precipitation present in tubing.  
 Y = GB carbide precipitation present in plate.

n = Practically no GB carbide precipitation in tubing.  
 N = Practically no GB carbide precipitation in plate.

i = Incomplete GB carbide precipitation in tubing.  
 I = Incomplete GB carbide precipitation in plate.

Figure 10. Effects of C & Si on Carbide Precipitation at 1600°F

As indicated in the Figure 8 T-T-T diagram, with longer time exposures in 1300-1800°F range, both Laves and Delta phase begin to precipitate. This precipitation begins in the grain boundary regions that already contain carbide particles. Figure 11 shows an example of this mixture of phases. The Delta phase is easy to identify because of its acicular morphology. The Laves particles, however, are very similar in morphology to the blocky, irregularly shaped  $M_6C$  and  $M_{23}C_6$  carbides. Thus it would be easy to overlook Laves particles in a metallographic examination. The diffraction pattern shown in Figure 11 and the chemical analysis given in Table III, both clearly indicate that Laves particles are present. Delta and Laves precipitation are shown as a single curve in the present T-T-T diagram. This may not be accurate in all cases, but to the extent that both phases rely upon the diffusion of Nb the kinetics of precipitation should be approximately the same for the two phases.

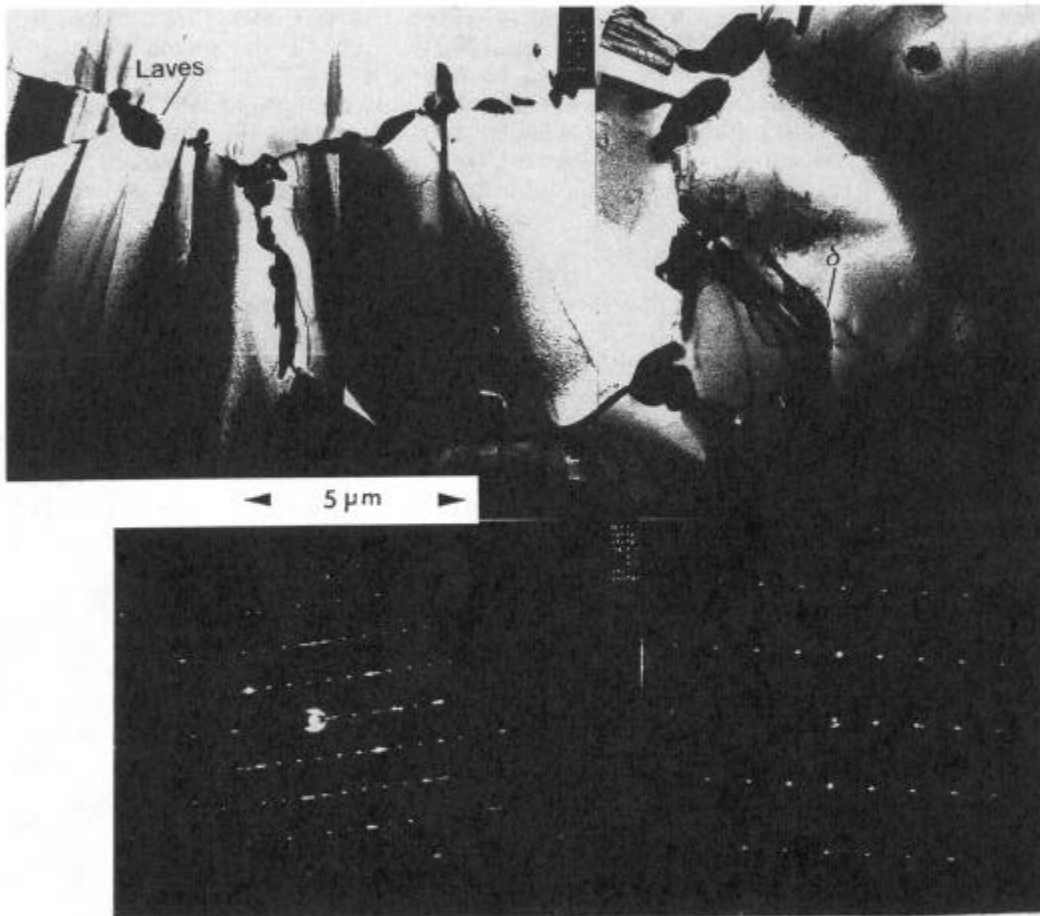


Figure 11. TEM Photographs of Laves and Delta Phases in A625 After 48 Hours Exposure at 1600°F

Grain boundary carbides, and also Delta and Laves particles can be put into solution by annealing at temperatures on the order of 2000°F or higher. At 2000°F grain boundary carbides will usually be eliminated by exposures on the order of an hour. Delta and Laves will also go into solution at 2000°F, but much longer annealing times are required. Annealing for 24 hours at 2000°F was necessary, for example, to completely dissolve the rather small quantities of Laves and Delta in the microstructure shown in Figure 11.

Thermal exposures in the 1400-1800°F range can degrade the ductility and toughness. This can become evident after even relatively short-time exposures, before Laves and Delta precipitates are formed. Table VIII shows the tensile properties after various thermal exposures of material that was subsequently age-hardened at 1200°F to raise the strength and thus magnify any effects of the thermal exposures. The tensile elongation and RA values dropped fairly significantly after thermal exposures of 4, 16, and 48 hours at either 1400, 1600, or 1800°F. Delta and Laves were observed only in the samples exposed 48 hours at 1400 or 1600°F. Thus the grain boundary carbides by themselves contributed significantly to the loss in ductility, even though the fractures in all cases were ductile, transgranular in appearance. Vernot-Loier and Cortial also noted that  $M_6C$  and  $M_{23}C_6$  particles reduced the ductility and impact energy of Alloy 625 (Reference 12).

Table VIII

Tensile Properties of A625 Heat After Various Thermal Exposures  
Material Initially Annealed 24 Hours at 2000°F, and Aged 24 Hours at  
1200°F After Thermal Exposure

<u>Exposure</u> <u>Temp.</u> <u>(°F)</u>	<u>Time</u> <u>(Hrs)</u>	<u>Yield</u> <u>Strength</u> <u>(ksi)</u>	<u>UTS</u> <u>(ksi)</u>	<u>Elong</u> <u>(%)</u>	<u>RA</u> <u>(%)</u>	<u>Laves &amp;</u> <u>Delta</u> <u>Particles</u>
1400	4	90.6	148.5	51	42	No
1400	16	93.0	153.1	46	42	No
1400	48	88.0	155.1	35	31	Yes
1600	4	84.7	143.7	50	39	No
1600	16	85.3	144.2	43	34	No
1600	48	83.4	141.0	32	44	Yes
1800	4	72.0	133.7	54	57	No
1800	16	75.0	135.5	53	52	No
1800	48	80.7	138.6	45	44	No

The earlier work of Kimball, et al, clearly demonstrated that Alloy 625 could become severely embrittled by thermal exposures of hundreds of hours in this temperature range (Reference 14). They also noted that the fracture appearance changed from ductile to intergranular with longer



exposure times. They attributed the embrittlement to precipitation hardening and the formation of brittle grain boundary phases. More recent work has confirmed these earlier tests. Figure 12 shows Kohler's (Reference 15) results in terms of iso-Charpy V-notch impact energy curves as a function of the exposure time and temperature. Kohler attributed the loss in toughness to the precipitation of Delta,  $\gamma''$  and carbide particles.

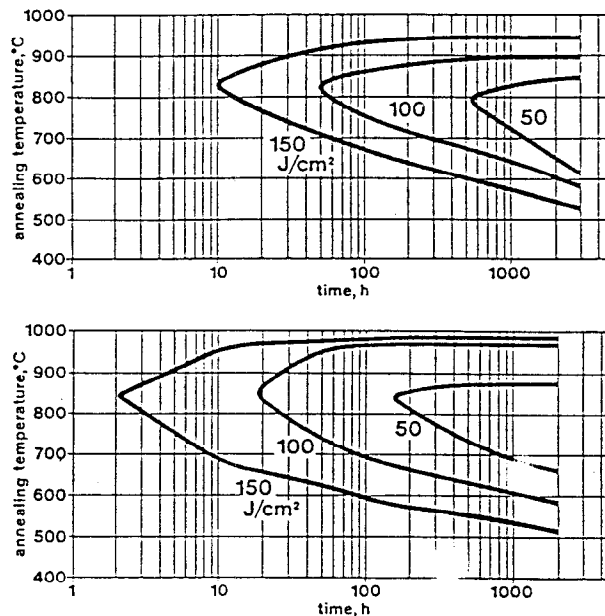


Figure 12. Effects of Thermal Exposures on the Impact Properties of Two Heats of A625 (Reference 15)

- Top: ISO-notch impact curves for lower Nb and C Alloy 625 heat annealed at 1120°C/50 min and aged as shown.
- Bottom: ISO-notch impact curves for "normal" Nb and C Alloy 625 heat annealed at 980°C/50 min and aged as shown.

As expected, reducing the C and Nb content will minimize the formation of the various grain boundary phases, and improve the resistance to thermal embrittlement. Figure 12 also shows Kohler's thermal embrittlement results with another heat of Alloy 625 in which the C was reduced from 0.03 to 0.011, and the Nb from 3.74 to 3.42 percent. This leaner composition was still embrittled, but the time to reach the same degree of embrittlement was increased by about a factor of three versus the higher C and Nb heat.

Thermal exposures also can markedly change the microstructures of weld metal or castings. Even if care is taken to avoid Laves phase in the as-cast structure, the enrichment in Nb in the interdendritic regions will lead to accelerated precipitation reactions upon heating. Figure 13 shows an example of Delta precipitation in GTA weld metal after 24 hours exposure at 1600°F. The Delta often could be seen to be localized in the

interdendritic regions of the weld structure. Figure 14 shows the effects of various thermal treatments on the appearance of Delta in this material, versus the T-T-T curve for Delta in wrought material. In this particular weld the time for Delta formation was reduced by a factor of about 50 versus the wrought material.

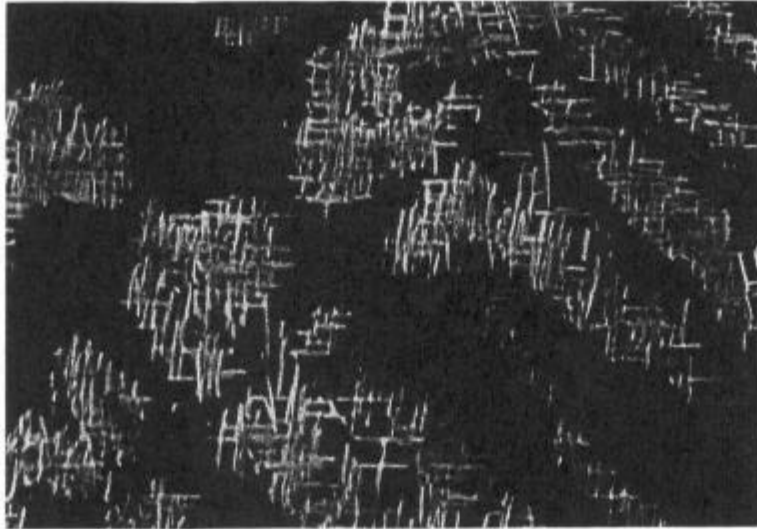


Figure 13. SEM Photograph of A625 Weld Metal After a Thermal Exposure of 24 Hours at 1600°F

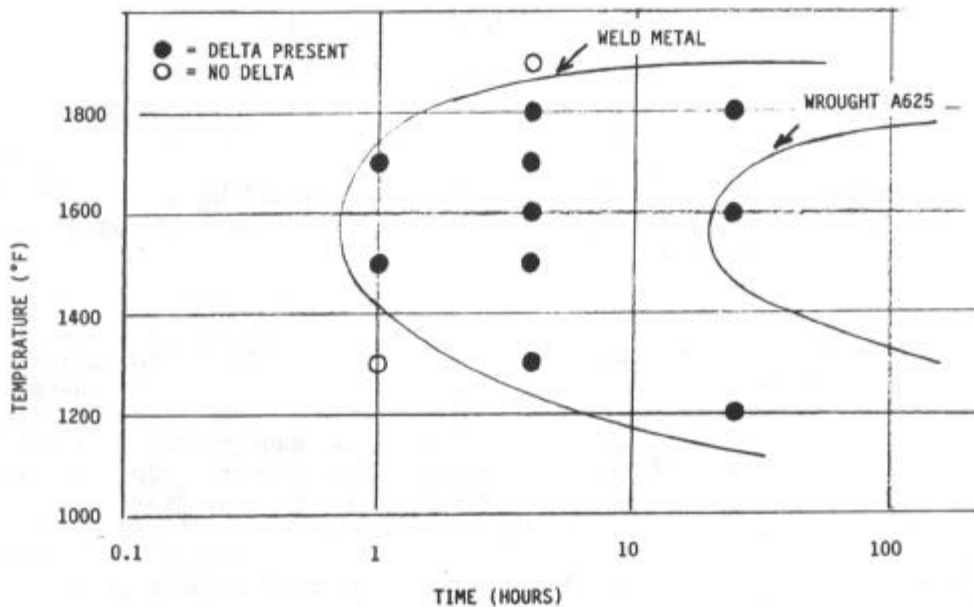


Figure 14. Thermal Exposure Conditions to Form Delta in Weld Metal Compared to Wrought A625

As expected, these precipitation reactions can adversely affect the toughness. In the weldment described above, the room temperature, Charpy V-notch impact energy decreased from 101.0 foot-pounds in the as-welded condition to 50.5 foot-pounds after the 1600°F/24 hour exposure. The precipitation reactions can be minimized by high temperature solution anneals to homogenize the structure and reduce the high local concentrations of Nb. This may be practical if the initial Nb segregation is not too severe. In large castings with extensive segregation, however, prolonged solution annealing may be impractical because excessive grain growth may take place.

Returning to the T-T-T behavior, at temperatures in the 1100-1400°F range, the precipitation of  $\gamma''$  is the dominating reaction. Alloy 625 was not originally developed as a precipitation hardened alloy, but with sufficient (Nb + Ti + Al) in the composition, significant  $\gamma''$  precipitation can take place. The general features of this reaction are very similar to those seen in Alloy 718, which was designed to be a precipitation hardened alloy. As shown in Table VII, the  $\gamma''$  phase is an ordered tetragonal I4/mmm structure that can be described chemically as  $Ni_3$  (Nb > 0.05, Ti < 0.5, Al < 0.5).

As shown in Figure 15, the  $\gamma''$  typically precipitates as reasonably uniformly distributed plate or disc shaped particles. With increasing time and temperature of the heat treatment, the particles will increase in length from approximately 0.01 to 0.1 microns.

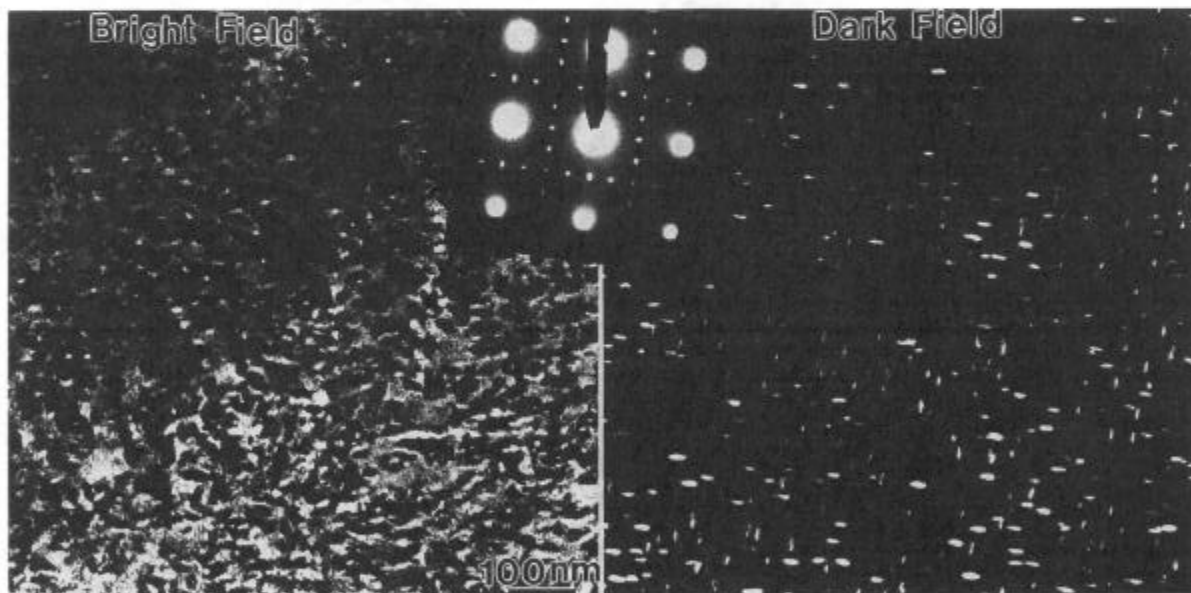


Figure 15. TEM Photographs of  $\gamma''$  Precipitate Particles in A625

Variations in processing history can produce many local variations in the precipitate morphology. Figure 16 shows the grain boundary region in material heat treated 90 hours at 1250°F that contains  $M_{23}C_6$  and NbC particles in the grain boundary and  $\gamma''$  extending up to the boundary with no apparent zone denuded of  $\gamma''$  adjacent to the grain boundary particles. As

shown in Figure 17, with variations in processing history  $\gamma''$  denuded zones around the grain boundaries can be found. One can find denuded zones around primary Nb particles, as seen in Figure 18, but here also the converse situation with no denuded zones can be found. The presence or absence of zones denuded in  $\gamma''$  probably reflects local variations in Nb content. If the local supply of Nb has been depleted by the formation of Nb-containing carbides, Laves or Delta particles in the area adjacent to these particles may be sufficiently depleted in Nb to retard the formation of  $\gamma''$ . The presence of denuded zones at the grain boundaries has often been associated with a degradation in mechanical properties or corrosion resistance in other precipitation hardened alloys. However, specific information on the effects of denuded zones in Alloy 625 is lacking. While one can generally explain why local denudation in  $\gamma''$  may be observed in Alloy 625, there is not yet sufficient information to define how the prior processing history affects the  $\gamma''$  precipitation behavior and resultant properties in Alloy 625.

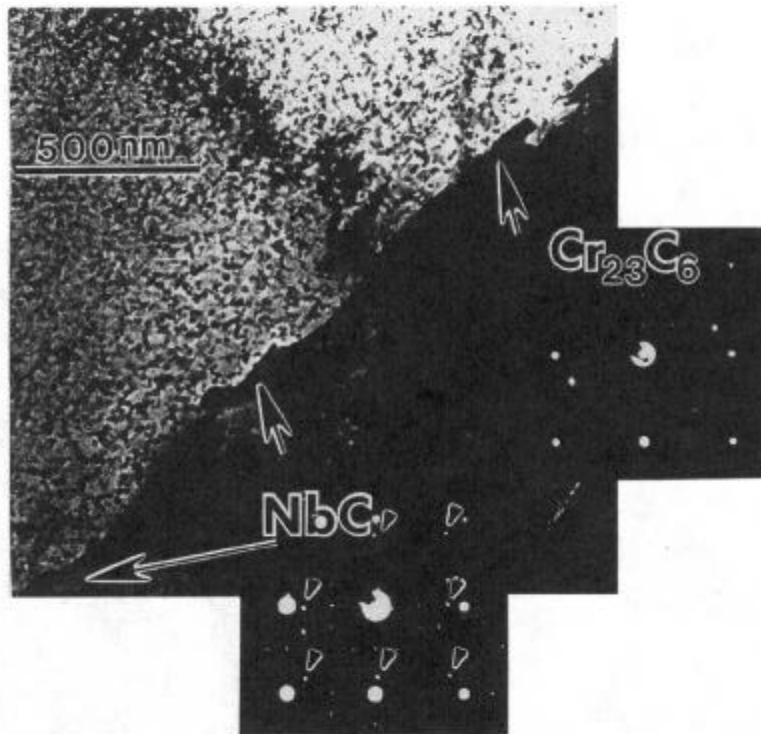


Figure 16. Precipitates at a grain boundary in the direct-aged A625

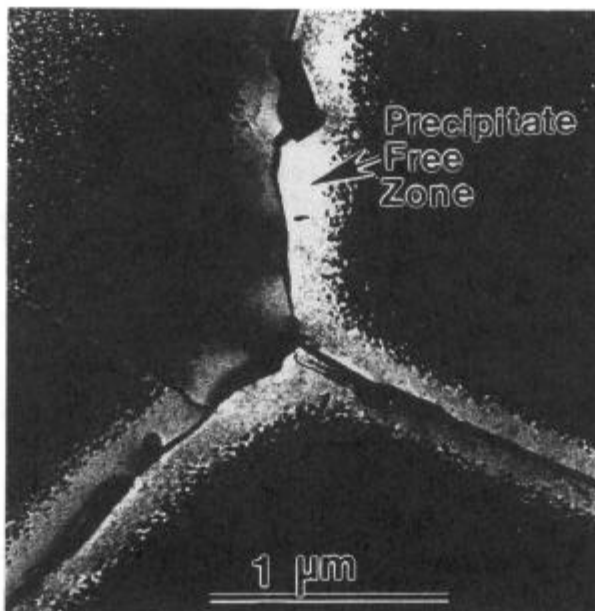


Figure 17. TEM Photograph of Precipitate Free Zone at Grain Boundaries of A625 After 24 Hours at 1400°F



Figure 18. (Nb, Ti)C particle in aged IN625 with  $\gamma''$  denuded around the carbide particle.

Alloy 625 is a marginal alloy for precipitation hardening purposes, and the  $\gamma''$  precipitation can be markedly altered by small changes in composition. Figure 19 shows the influence of the Ti content in series of small lab melts that all contained approximately 3.85% Nb and were otherwise nominally constant in composition. Reducing the Ti from 0.4 to 0.05 and then to 0 percent significantly retarded the precipitation of  $\gamma''$ . As shown in Figure 20, reducing the Al to zero had much less effect. Microstructural examinations showed that only  $\gamma''$  was involved in the precipitation hardening in these tests. No  $\gamma'$  or other phases that could contribute to the hardening were detected. Similar effects of alloy chemistry have been observed by Garzarolli et al (Reference 16). Consistent with the present results, they postulated that the individual effects of Nb, Al, and Ti can be explained in terms of precipitation of an  $Ni_3(Al + Ti + Nb)$   $\gamma''$  precipitate.

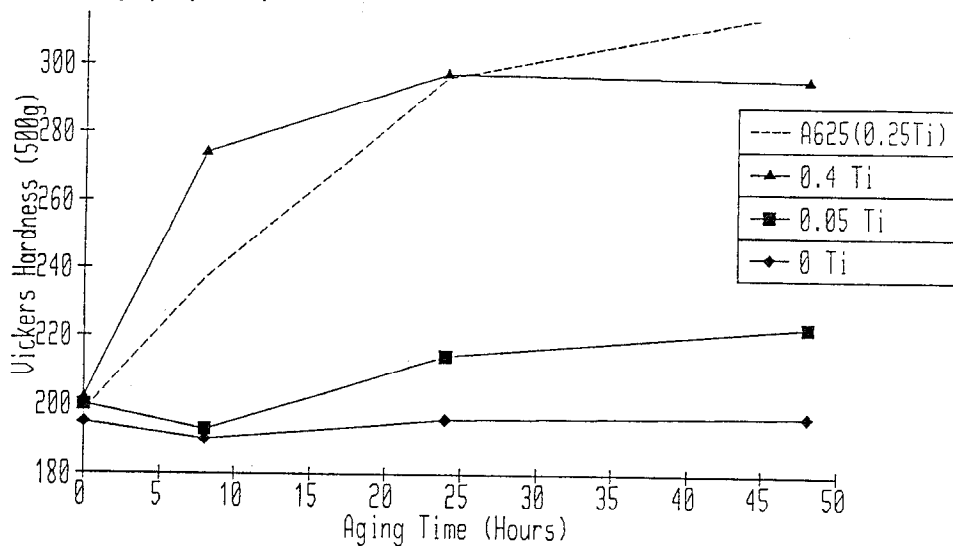


Figure 19. Effects of Ti Content on the Age Hardening Behavior of A625 at 1200°F

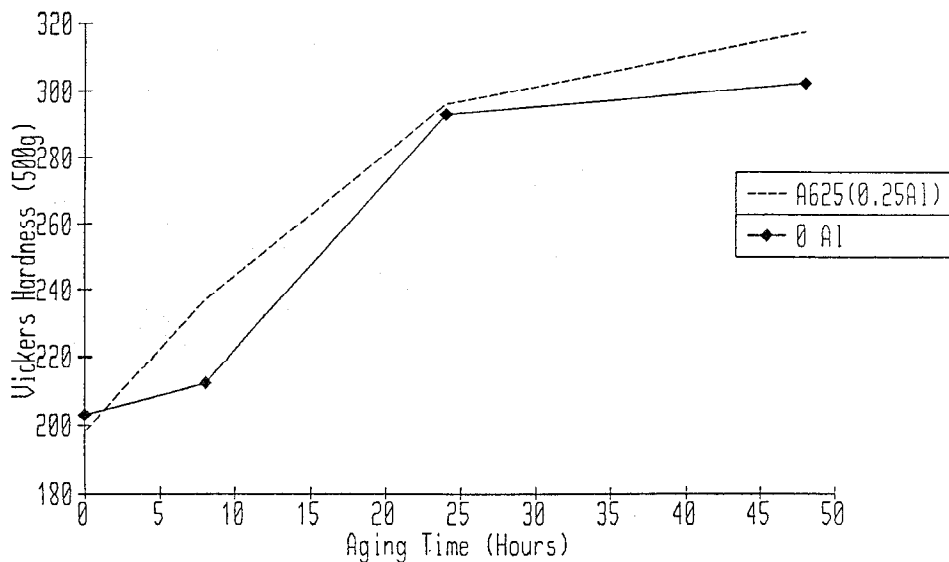


Figure 20. Effects of Al Content on the Age Hardening Behavior of A625 at 1200°F

## COMPOSITIONAL FINE TUNING

The structures and properties of individual heats of Alloy 625 can vary considerably depending upon the processing history and chemical composition of the heat. Depending upon the intended properties and application, it may often be advisable to use more restrictive compositional limits than those given in Table I, so as to ensure consistent properties on a heat-to-heat basis. To do this successfully, however, requires some consideration of the various trade-offs in properties that may result when such compositional modifications are made.

One step in this process is to consider how compositional changes affect the microstructure. Table IX attempts to summarize some of the compositional effects discussed in the preceding pages. Phase formation during solidification and during heat treating are both considered.

Table IX

### Effects of Alloying Elements on Formation of Phases During Solidification on During Heat Treatment

Element	Minimize Formation of NbC During Solidification	Minimize Formation of Laves Phase During Solidification	Minimize Carbide Precipitation During Heat Treatment	Minimize Laves and Delta Precipitation During Heat Treatment	Avoid $\gamma''$ Precipitation
Minimize Nb	Helps	Helps	Helps	Helps	Helps
Minimize Fe	N	Helps	N	N	N
Minimize Mo	N	Helps	Helps	Helps <sup>(2)</sup>	N
Minimize Ti and Al	N	N	N	N	Helps
Minimize C	Helps	Hurts <sup>(1)</sup>	Helps	N	N
Minimize Si	N	Helps	Hurts	Helps <sup>(2)</sup>	N

N = No significant effect, or effect not certain.

(1) = Lower C/Nb ratio probably outweighs effect of minimizing solidification range.

(2) = Low Mo or Si would retard Laves, have little effect on Delta.

Laves and NbC particles formed during solidification, and Laves and Delta particles formed during heat treating are detrimental phases that generally should be avoided. Certain types and distributions of grain boundary carbides, however, may be beneficial for stress corrosion resistance in certain environments, and  $\gamma''$  is necessary if high strengths are desired. Thus, the first step in tightening a composition range would be determine if grain boundary carbides and/or  $\gamma''$  precipitation hardening are required.

A further step is to consider the roles of the various alloying elements on the important material properties. Table X shows a very simplified way of considering how changing the composition would tend to affect the mechanical properties, corrosion resistance and weldability of Alloy 625. For specific applications much more detail will usually be necessary to accurately evaluate the effects of compositional variations on the

properties of concern. Indeed for certain specific cases it is likely that some of the generalized conclusions in Table 10 may be inappropriate. The principal point to be made here is that fine tuning the composition requires a consideration of all the consequences of the composition change to ensure that solving one problem does not create a new one.

A final consideration is cost. Overly restrictive chemistry ranges can be expensive, and should not be imposed if not necessary.

Table X

Some General Effects of Alloying Elements on Properties of Alloy 625

Element	Strength	Corrosion Resistance	Weldability
Minimize Nb	Hurts	N	Helps
Minimize Fe	Hurts	N	Helps
Minimize Mo	Hurts	Hurts	Helps
Minimize Ti and Al	Hurts <sup>(1)</sup>	N	Hurts <sup>(2)</sup>
Minimize C	N	Hurts <sup>(3)</sup>	Helps
Minimize Si	N	Hurts <sup>(3)</sup>	Helps

N = No significant effect, or effect not certain.

<sup>(1)</sup> = Ti and Al will be important to strength only if precipitation hardening is employed.

<sup>(2)</sup> = Some amounts of Ti and Al are helpful to weldability. Minimum levels required are not known.

<sup>(3)</sup> = If grain boundary carbides are necessary for corrosion resistance, some minimum C and Si levels will be needed. See Figure 10.

**SUMMARY**

Although designed as a "simple" solid solution alloy, Alloy 625 is not a simple material. A variety of different phases can be produced in Alloy 625 during solidification or during thermal processing. Some of these phases, particularly Laves and Delta, have only detrimental effects, and should be avoided. Others, such as grain boundary carbides and  $\gamma'$ , can be helpful for corrosion resistance or strength purposes. A potential problem for people who use Alloy 625 is that the composition range is overly broad, and widely different properties may be found in different heats of this alloy. Tightening the composition range to meet specific application goals should help ensure more consistent heat-to-heat results. However, some care is needed in these composition modifications to ensure that some important property is not compromised, and that the costs to produce an overly narrow composition range do not become excessive.



All of this is, of course, very familiar to those who work with Alloy 718. Indeed, most of what has been said here could, with some adjustments, be said of Alloy 718. People who use Alloy 718 have learned how to adjust the composition and processing steps in order to achieve consistently satisfactory properties, and Alloy 625 users may benefit from this experience and take similar steps.

#### REFERENCES

1. H. L. Eiselstein ASTM STP No. 369, 1965, p. 62.
2. B. Radhakrishna and R. G. Thompson Met Trans Vol. 22A, 1991, p. 887.
3. M. J. Cieslak, T. J. Headley, T. Kollie and A. D. Romig Met Trans Vol. 19A, 1988, p. 2319.
4. S. M. Jones, J. F. Radavich and S. Tian "Superalloy 718", TMS, 1989, p. 589.
5. E. L. Raymond "Superalloy 718" TMS 1989, p. 577.
6. M. J. Cieslak Weld Journal Vol. 70, 1991, p. 49S.
7. I. L. W. Wilson, R. G. Gourley, R. M. Walkosak, G. J. Bruck "Superalloys 718, 625", TMS, 1991, p. 735.
8. M. J. Cieslak, G. A. Knorovsky, T. J. Headley and A. D. Romig Met Trans Vol. 12A, 1986, p. 2107.
9. C. Chen, R. G. Thompson and C. W. Daves "Superalloys 718/625", TMS, 1991, p. 81.
10. G. Chen, Q. Zhu, D. Wang, X. Xie, and J. F. Radavich "Superalloys 718/625", TMS, 1991, p. 545.
11. R. Cozar, M. Rouby, M. Mayonobe and C. Morizot "Superalloy 718/625" TMS 1991, p. 423.
12. C. Vernot-Loier and F. Cortial "Superalloy 718/625", TMS, 1991, p. 409.
13. L. Ferrer, B. Pieraggi and J. F. Ugmet, "Superalloys 718/625", TMS, 1991, p. 217.
14. G. F. Kimball, W. R. Pieren and D. J. Roberts, Presented at ASME Annual Winter Meeting, Detroit, MI, November 1973.
15. M. Kohler, "Superalloys 718/625", TMS, 1991, p. 363.
16. F. Garzarolli, A. Gersha, and K. P. Francke, Zeit. Metalk. Vol. 60, 1969, p. 643.